Chemical potential shift of $Fe_{3-x}V_xSi$ studied by hard x-ray photoemission

Y. T. Cui,[1,*] A. Kimura,[1,†] K. Miyamoto,[1] M. Taniguchi,[1,2] T. Xie,[2] S. Qiao,[2,3] K. Shimada,[2] H. Namatame,[2] E. Ikenaga,[4] K. Kobayashi,[5] Hsin Lin,[6] S. Kaprzyk,[7] A. Bansil,[6] O. Nashima,[8] and T. Kanomata[8]

[1]*Graduate School of Science, Hiroshima University, Higashi-Hiroshima 739-8526, Japan*

[2]*Hiroshima Synchrotron Radiation Center, Hiroshima University, Higashi-Hiroshima 739-0046, Japan*

[3]*Advanced Materials Laboratory, Physics Department and Surface Physics Laboratory, Fudan University, Shanghai 200433, China*

[4]*Japan Synchrotron Radiation Research Institute, SPring-8, Sayo, Hyogo 679-5198, Japan*

[5]*National Institute for Materials Science, SPring-8, Sayo, Hyogo 679-5198, Japan*

[6]*Department of Physics, Northeastern University, Boston, Massachusetts 02115, USA*

[7]*Department of Physics, Northeastern University, Boston, Massachusetts 02115, USA and Faculty of Physics and Nuclear Techniques, Academy of Mining and Metallurgy, al. Mickiewicza 30, 30-073 Kraków, Poland*

[8]*Faculty of Engineering, Tohoku Gakuin University, Tagajo 985-8537, Japan*

(Received 6 May 2008; revised manuscript received 21 July 2008; published 19 November 2008)

Core-level photoemission spectra of $Fe_{3-x}V_xSi$ alloys with inequivalent Fe_I and Fe_{II} sites are investigated via hard x-ray photoemission spectroscopy over the entire doping range $x=0-1$. All the measured 1*s* core-level peaks are found to shift to higher binding energy with increasing V concentration. First-principles, all electron charge- and spin-self-consistent electronic structure computations within the framework of the local-spin-density approximation are used to interpret the experimental results. The measured size of energy shift in going from $x=0$ to 1 is consistent with the corresponding theoretical value for the Fe_{II} and Si 1*s* core levels, whereas for the Fe_I and V core levels the computed shifts are generally larger than the experimental values. We ascribe these discrepancies to the effects of the core-hole screening in the final state which are not accounted for in the computations. In a rigid-band model the chemical potential and the core-level binding energies are expected to *decrease* with V doping as electrons are depleted from the Fermi energy. The observed *increase* in the binding energy of core levels thus supports a picture of the electronic structure where V doping induces a "pseudogap" or a region of reduced density of states in the vicinity of the Fermi energy.

DOI: 10.1103/PhysRevB.78.205113 PACS number(s): 71.20.Lp, 79.60.−i

I. INTRODUCTION

Fe_3X (X is a metalloid such as Al, Si, and Ga) and the related compounds $Fe_{3-x}Y_xX$ (Y is a transition metal) have attracted experimental[1–6] and theoretical[7–10] attention in view of their half-metallic electronic structure (Fe_2MnX,[11] Co_2MnX,[12,13] etc.) and useful properties such as the ferromagnetic shape memory effect [Ni_2MnGa (Ref. 14)] and magnetoresistance [$Ni_{50}Mn_{36}Sn_{14}$ (Ref. 15)]. These Heusler-type compounds have also been investigated recently as thermoelectric materials due to the possible formation of a pseudogap[16] in the electronic density of states (DOS) near the Fermi level E_F.[2,4,5] The reason is that the Seebeck coefficient S at temperature T is given in terms of the density of states $N(E)$ by[17]

$$S = -\frac{\pi^2}{3}\frac{k_B^2 T}{e}\frac{1}{N(E_F)}\left[\frac{\partial N(E)}{\partial E}\right]_{E=E_F}. \quad (1)$$

The presence of a sharp pseudogap in the vicinity of E_F may then lead to enhancement of the Seebeck coefficient, and a change in its sign, when the E_F moves through the pseudogap region as illustrated schematically in Fig. 1. This suggests that one could manipulate thermoelectric properties of materials through chemical substitution on specific sites as a way of adjusting the formation of the pseudogap and/or the position of the E_F in relation to the minimum in the DOS. In this connection $Fe_{3-x}V_xSi$ ($0 \le x \le 1$) alloys with relatively high thermoelectric power (TEP) (see, e.g., Refs. 2 and 4) constitute a relatively simple test case.

The pseudobinary compound Fe_3Si possesses the DO_3 crystal structure as shown in Fig. 2—an fcc Bravais lattice with four basis atoms: Fe_{II} (A and C), Fe_I (B), and X (D) sites. Fe_I atoms sit at the center of a cube with eight Fe_{II} nearest neighbors at the corners, the local symmetry being that of bcc iron. Fe_{II} sites have four nearest-neighbor Fe_I atoms and four neighboring X atoms in tetrahedral coordination. The X sites are surrounded by eight nearest-neighbor Fe_{II} atoms. Since there are two inequivalent Fe sites in Fe_3Si with different local coordinations, Fe_3Si may be represented as $(Fe_I)(Fe_{II})_2Si$, which has the form of the basic unit cell of Heusler-type alloys except that the two different sites are occupied by Fe atoms. V impurities in the alloy preferentially occupy Fe_I site.[6,18]

Experimental studies[2,4] suggest that the substitution of Fe by V in Fe_3Si causes the formation of a pseudogap around the Fermi energy. Electronic structure computations[7,8] indi-

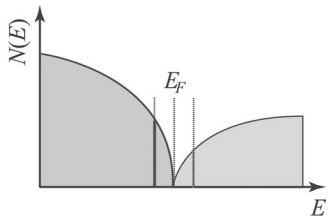

FIG. 1. Schematic density of states depicting a sharp pseudogap around E_F, which could lead to an enhancement of the Seebeck coefficient and a change in its sign depending on the placement of the E_F.

 ©2008 The American Physical Society

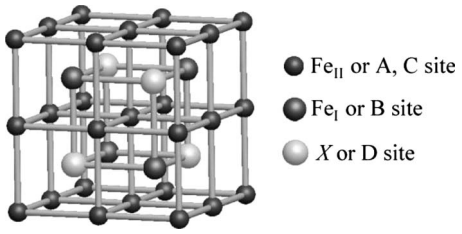

FIG. 2. Crystal structure of Fe_3X.

cate that with increase in V concentration, the Fermi level moves to higher energy and a pseudogap in the DOS develops at large x together with a decrease in the total magnetic moment. This trend is opposite to what is expected from a rigid-band picture and shows that the electronic structure changes significantly with increasing V content. It is important therefore to establish how the chemical potential evolves in this system with V doping. To our knowledge, no direct evidence for chemical potential shift (CPS) has been demonstrated experimentally. Since the binding energies in photoemission spectra are measured with respect to the chemical potential μ (i.e., the Fermi level), the binding energy of characteristic features in photoemission spectra should shift when the chemical potential changes. It has been reported[19] that the observed Si $2p$ core-level shifts arise from a CPS, limitations of surface sensitivity of the vacuum-ultraviolet (VUV) spectra notwithstanding. Fortunately, recent advances in x-ray undulator technology at third-generation synchrotron light sources enable the delivery of unprecedented high photon flux,[20,21] which can well compensate for the suppression of cross section and analyzer transmission, and make high-energy, high-resolution x-ray photoemission spectroscopy (XPS) accessible. The longer escape depth of photoelectrons with higher kinetic energy will facilitate electronic structure studies of bulk materials, nanoscale buried layers, and their interfaces since the relative contribution of signal from the surface region is reduced.[22,23] So motivated, we have measured the core-level photoemission spectra of $Fe_{3-x}V_xSi$ using hard x-ray photoelectron spectroscopy (HXPES). The present paper discusses how one can adduce CPS from the measured binding-energy shifts in light of the corresponding electronic structure computations.

II. EXPERIMENT

$Fe_{3-x}V_xSi$ polycrystalline samples were prepared by repeated arc melting of mixtures of 99.99% pure Fe and Si, and 99.9% pure V under purified argon atmosphere. The subsequent postannealing was performed at 1123 K for 5 days to improve the homogeneity of the alloys. X-ray powder-diffraction patterns of $Fe_{3-x}V_xSi$ ($0 \leq x \leq 1$) and Fe_2VSi contained only the diffraction lines expected for the DO_3 and $L2_1$ structures, respectively.

The photoemission experiments were carried out with synchrotron radiation in the hard x-ray region at the undulator beamline BL-29XU of SPring-8. The x rays ($h\nu = 7936$ eV) monochromatized by a Si (111) double-crystal monochromator were vertically focused by a cylindrically bent mirror onto the samples mounted in an analyzer chamber. A hemispherical electron analyzer with multidetection system (Gammadata Scienta R4000) modified to accommodate photoelectrons with high kinetic energies up to 8 keV was used. The angle between the incident photon beam and the lens axis of the analyzer was 90°. At the same time, the acceptance angle of the analyzer was set to ±8°. The position of the Fermi level and the total-energy resolution were checked with the evaporated Au film. Besides, in order to calibrate and confirm the excitation energy, the Au $4f$ lines were also measured frequently. The vacuum of the analyzer chamber was $\sim 3 \times 10^{-8}$ Pa during the measurements. The clean surfaces of the specimens were obtained by *in situ* fracturing with a knife edge in ultrahigh vacuum chamber. The evaluated total-energy resolution was about 200 meV for $h\nu = 7936$ eV at a sample temperature of 35 K.

III. RESULTS AND DISCUSSION

Figure 3 shows the Fe, V, and Si $1s$ core-level spectra of $Fe_{3-x}V_xSi$ for various x's. The spectra were deconvoluted with Doniach-Šunjić functions after subtracting a Shirley-type background. Notably, Si $1s$ core levels can be fitted well with a relatively symmetric peak, while Fe $1s$ spectra cannot be fitted with a single symmetric function, especially for small x due to the enhancement of full width at half maximum (FWHM). The broadening of V $1s$ spectra with increasing x also indicates that an additional component contributes to the spectrum. For these reasons, Fe and V $1s$ spectra have been fitted with two asymmetric peaks (marked A and B). The fitted results are plotted in Fig. 3 and the fitting parameters are listed in Table I.

One can observe clearly in Fig. 3 a shift of all the main $1s$ lines to higher binding energy with increasing x. The Fe and V $1s$ binding energies of the intensity maxima as well as the fitted peak positions are plotted in Fig. 4. The fitted peak positions for both peaks A and B show the same trend as the binding energies assigned via the intensity maxima. Note that the fitted peak positions of peak A are nearly the same as the binding energies assigned with the intensity maxima due to the small contribution of peak B. Therefore, hereafter we will only use the binding energies assigned with the intensity maxima.[24] For a more detailed analysis, the relative binding energies (E_B) of $1s$ and $2p$ core lines of Fe, V, and Si, as well as the calculated chemical potentials as a function of x, are shown in Fig. 5(a). Here, the Si $2p$ core-level data are taken from Ref. 19 using VUV light. Also, the binding energies of V core levels have been extrapolated by making a linear fit using data from $x=1$ to 0. Although the size of the core-level shifts is seen to be different for various elements and to vary for different orbitals of the same atom, the most important point to note is that all the core levels shift toward higher binding energy with increasing x in more or less the same way.

It is useful to recall that the binding-energy shift $\Delta E_B'$ (measured relative to the chemical potential μ) can be expressed as[25–29]

$$\Delta E_B' = \Delta\mu - K\Delta Q + \Delta V_M - \Delta E_R \qquad (2)$$

in terms of the chemical potential change $\Delta\mu$. Here, ΔQ is the change in the number of valence electrons on the atom,

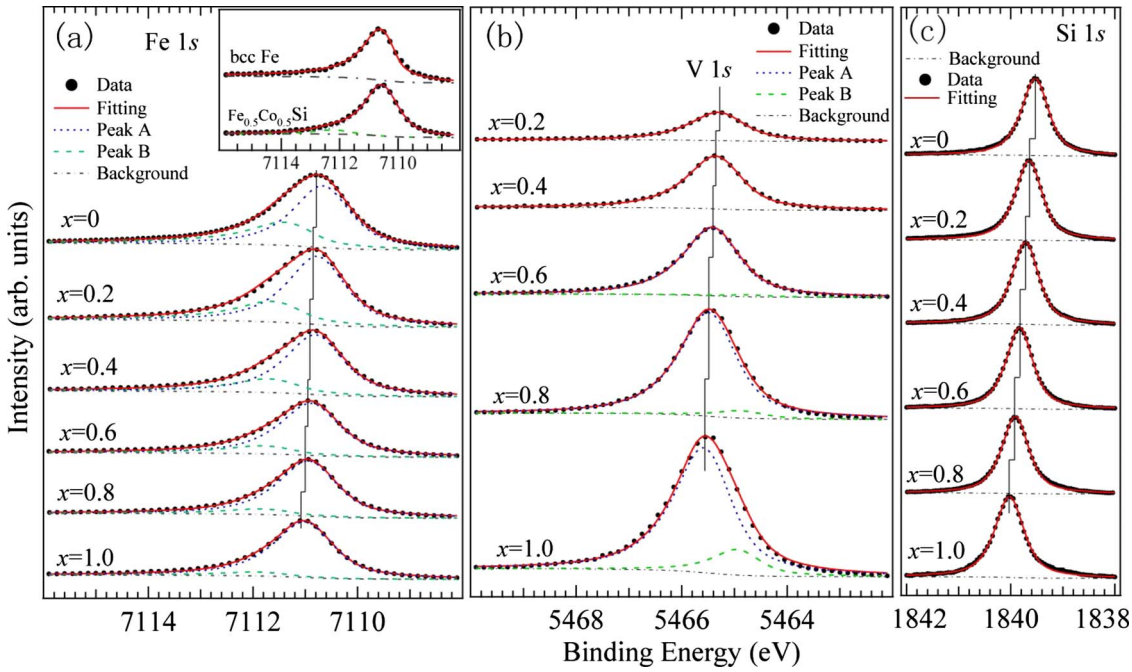

FIG. 3. (Color online) Raw data and fits for (a) Fe, (b) V, and (c) Si 1*s* core-level photoemission spectra of $Fe_{3-x}V_xSi$ for various *x*'s. The peak positions in raw data are marked by vertical lines. The spectra have been deconvoluted using Doniach-Šunjić functions after subtracting a Shirley-type background. The fitting parameters are listed in Table I. The inset shows Fe 1*s* spectra of bcc Fe and $Fe_{0.5}Co_{0.5}Si$ and the corresponding fits for reference.

which produces changes in the electrostatic potential at the core-hole site as well as in the intra-atomic relaxation energy of the core-hole final state. ΔQ depends on valence and is usually called the chemical shift. K is a coupling constant between core and valence electrons. ΔV_M is the change in the Madelung potential and ΔE_R is the change in the relaxation energy. ΔQ and ΔV_M which involve electronic and ionic potentials are initial-state effects. The term ΔE_R takes into account the final-state effects resulting from the adaption of the system to the presence of the core hole after photoionization.

In order to understand the observed core-level shifts, we have computed the core-level binding energies of Fe_I, Fe_{II}, V, and Si atoms in $Fe_{3-x}V_xSi$, which are presented in Figs. 4 and 5. The computations were carried out using the fully charge- and spin-self-consistent, all electron Korringa-Kohn-Rostoker coherent-potential approximation (KKR-CPA) disordered alloy methodology within the framework of the local spin density approximation (LSDA) for $x=0.25$, 0.50 and 0.75, together with the limiting cases of the end compounds Fe_3Si and Fe_2VSi. The core states were treated relativistically and the valence states semirelativistically.[30] For further details of the computations we refer to Ref. 7. In terms of Eq. (2), note that our calculated core-level shifts automatically include not only the effects of the chemical potential shifts but also those of the chemical shifts and Madelung potentials. Differences between the chemical environments of various sites lead to differences in the theoretical core-level shifts. We see from Fig. 4 that while both Fe_I and Fe_{II} 1*s* core levels shift to higher binding energy with V concentration, the size of the shift is slightly smaller for Fe_{II}. Similarly, the binding energy of the computed Fe_I and Fe_{II} $2p_{3/2}$ levels in Fig. 5(b) increases more or less monotonically, although the curve for the Fe_{II} shift is seen to be rather flat between $x=0$ and $x=0.25$. The calculated V core levels show the largest shift among the three elements [see Fig. 5(c)], a shift comparable to the CPS (~ 1 eV for $x=1$).[31] Finally, the predicted Si core-level shifts in Fig. 5(d) show a different behavior from other sites in that the size of the shift is substantially smaller than for Fe and V, and like the Fe_{II} $2p_{3/2}$ level, there is relatively little shift over $x=0$ and 0.25.

The experimentally observed binding-energy shift of Fe core levels are seen in Fig. 5(b) to be similar to the theoretical results for Fe_{II} although the size of the shift from $x=0$ to 1 for Fe 1*s* is somewhat smaller in the experiment (0.4 eV) compared to that in the calculations (0.55 eV). Since the peak maxima of Fe 1*s* spectra are dominated by Fe_{II} contribution (namely, Fe 1*s* peak *A*, which will be proved later), the experimental results are thus essentially consistent with theoretical predictions. It is here noticed that the magnitude of Fe 1*s* core-level shift is a little smaller than that of Fe $2p_{3/2}$, which might be due to a little enhanced surface sensitivity in the lowered electron kinetic energy of photoelectrons from Fe 1*s* core level. In contrast, the theoretical 1*s* shifts for Fe_I and V, which amount to 0.7 and 1 eV, respectively, are substantially larger than the corresponding experimental values. For the Si 1*s* core level, however, a reasonable agreement is found between theory and experiment, although the size of the theoretical shift (0.35 eV at $x=1$) is a little smaller than experimental one (0.5 eV). Interestingly, the computed shift in the energy of the V core levels is quite similar in size to the estimated chemical potential shift ($\Delta\mu$), while shifts of Fe and Si levels are much reduced from $\Delta\mu$. These results show clearly that the core-level shifts in general involve significant contributions not only from the CPS

TABLE I. Parameters obtained from the best fit of Fe, V, and Si 1*s* core-level photoemission spectra of $Fe_{3-x}V_xSi$ for various x values, and for Fe 1*s* spectra of bcc Fe and $Fe_{0.5}Co_{0.5}Si$. Peaks are fitted using Doniach-Šunjić functions after subtracting a Shirley-type background.

Core level	Peak		x=0	x=0.2	x=0.4	x=0.6	x=0.8	x=1.0
Fe 1*s*	*A*	E_B (eV)	7110.67	7110.77	7110.81	7110.89	7110.94	7111.02
		FWHM(eV)	1.31	1.33	1.34	1.37	1.35	1.36
		Asymmetry α	0.10	0.10	0.10	0.10	0.10	0.10
	B	E_B (eV)	7111.40	7111.64	7111.69	7111.81	7111.84	7111.92
		FWHM(eV)	1.55	1.56	1.57	1.57	1.55	1.57
		Asymmetry α	0.40	0.40	0.40	0.40	0.40	0.40
		Peak *B*-*A* ratio	0.50	0.40	0.30	0.20	0.13	0.09
V 1*s*	*A*	E_B (eV)		5465.31	5465.36	5465.42	5465.48	5465.59
		FWHM(eV)		1.25	1.25	1.27	1.30	1.32
		Asymmetry α		0.13	0.13	0.13	0.13	0.14
	B	E_B (eV)				5464.74	5464.89	5464.95
		FWHM(eV)				1.10	1.10	1.10
		Asymmetry α				0.13	0.13	0.14
		Peak *B*-*A* ratio				0.03	0.06	0.17
Si 1*s*		E_B (eV)	1839.53	1839.65	1839.72	1839.83	1839.91	1840.02
		FWHM(eV)	0.62	0.61	0.61	0.61	0.62	0.67
		Asymmetry α	0.06	0.06	0.05	0.05	0.04	0.03

Sample	Core level	Peak	E_B (eV)	FWHM(eV)	Asymmetry α	Peak *B*-*A* ratio
bcc Fe	Fe 1*s*		7710.617	1.37	0.4	
$Fe_{0.5}Co_{0.5}Si$	Fe 1*s*	*A*	7110.577	1.42	0.1	
		B	7112.227	1.50	0.1	0.1

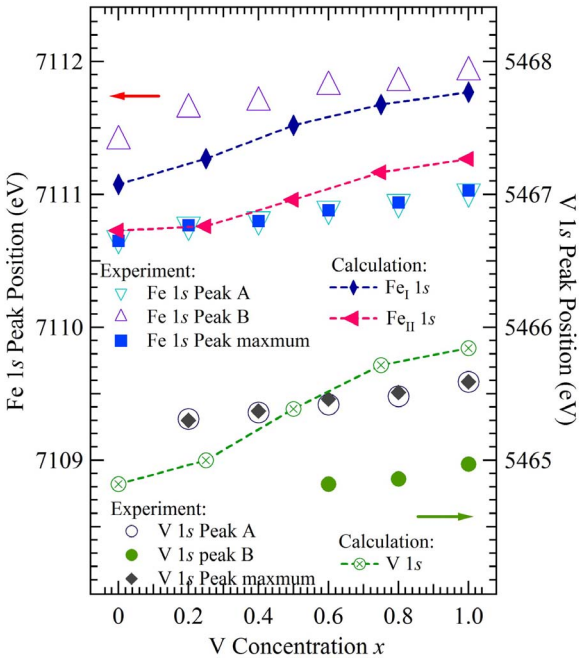

FIG. 4. (Color online) Comparison of the Fe and V 1*s* core-level binding energies at the intensity maxima, the fitted peak positions, and the corresponding computed binding energies as a function of the V concentration x. Theoretical binding energies have been shifted by 201 eV for Fe and 159.5 eV for V, independent of x.

but also from chemical shifts and changes in the Madelung potential.

The discrepancies between theory and experiment seen in Figs. 4 and 5 are due presumably to the fact that the relaxation energy contribution E_R of Eq. (2) has not been accounted for in our computations. The relaxation energy reflects the effects of charge rearrangements in the solid, which result when the core hole suddenly appears in the photoexcitation process and the surrounding electrons move to screen this positive charge.[25,26] This response, which entails intra-atomic as well as interatomic electronic relaxations, can be expected to vary with doping as the chemical environment and/or the electron density changes. The nearly symmetric line shape of the Si 1*s* spectrum in Fig. 3 suggests that the effects of metallic screening on Si core levels are small, while this is not the case for V and Fe sites. Although we have not attempted to model the relaxation energy and the even more delicate changes therein induced by doping, further analysis of the data of Figs. 4 and 5 in this regard should prove worthwhile.

The observed trends in core-level binding energies with increasing x cannot be understood within the rigid-band picture because V has less valence electrons than Fe. Therefore, if the rigid-band picture holds, when Fe is substituted by V, the chemical potential would be lowered as shown in Fig. 6(b), with a concomitant lowering of the core-level binding energy. This however is in sharp contrast to the experimental as well as theoretical results of Figs. 4 and 5, where all the

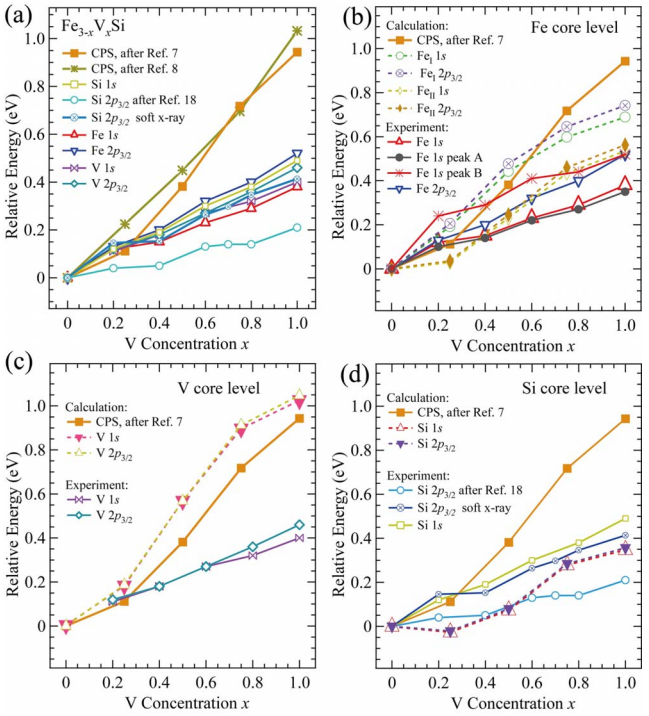

FIG. 5. (Color online) (a) Energy shifts in $Fe_{3-x}V_xSi$ relative to those in Fe_3Si ($x=0$) as a function of x. Experimental binding energies refer to the intensity maxima (Ref. 24). Binding energies of V core levels are extrapolated linearly using data from $x=1$ to 0. [(b)–(d)] Comparison of experimental and theoretical results for 1s and 2p core-level binding energies of Fe, V, and Si as indicated in the legends.

core levels essentially show an *increase* in binding energy with V doping. Figure 6(c) illustrates how when a pseudogap forms and the states around the Fermi energy are depleted, the chemical potential can rise with increasing V content even when the total number of valence electrons in the system decreases. The formation of the pseudogap and the associated CPS is thus the main reason for the core-level shifts in Figs. 4 and 5. Further insight is provided by the spin-resolved energy-level diagrams at Γ ($k=0$) and the partial d

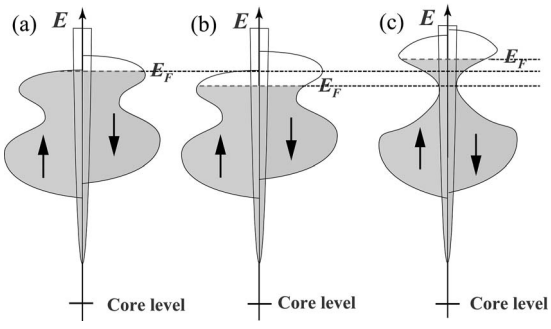

FIG. 6. Schematic diagrams illustrating chemical potentials in various cases. (a) Fe_3Si; (b) rigid-band scenario when Fe is substituted by V and the electron density is reduced; (c) effect of pseudogap formation, where despite a reduction in valence electrons the chemical potential is pushed to higher energy due to the reduced DOS below the Fermi energy.

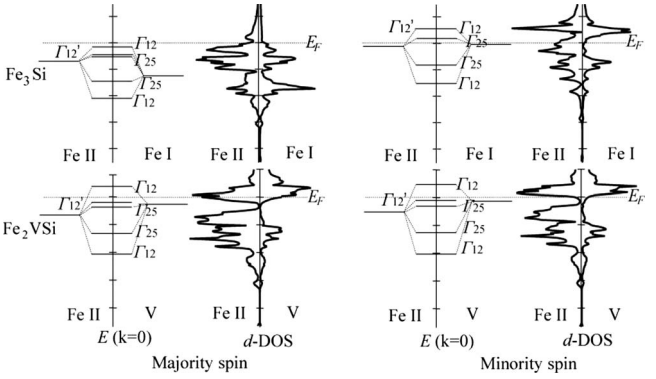

FIG. 7. Energy-level diagrams at Γ ($k=0$) together with the partial d DOS of Fe and V in Fe_3Si (upper) and Fe_2VSi (lower). Results for majority- (right) and minority-spin (left) components are given in each case. Symmetry labels are after Ref. 32.

DOSs (after Ref. 7) of Fe and V in Fe_3Si and Fe_2VSi, which are given in Fig. 7. The d orbitals of Fe_I and V will mix with those of Fe_{II} of the same symmetry. As a result, the partial DOS of Fe_{II} undergoes substantial changes with doping due to interactions with V and Fe_I. The splitting between Γ_{12} and Γ_{25} states is small in Fe_3Si. As the V concentration increases, the d DOSs of Fe_{II} evolve to form a deep valley around the Fermi level, much like Fe_2VSi where a gap appears in both spins. In other words, with increasing V content, the highest occupied states near the Fermi level are pushed to higher energies, which deepen the dip in the DOS and pushes the chemical potential to higher values for both spins. Even though V is more electropositive than Fe, the reduction in valence electrons due to V addition is not enough to compensate for the reduction in DOS below the Fermi level. A similar discussion can also be found elsewhere.[7,11,33,34]

Finally, we consider the origin of peaks A and B in the Fe 1s core-level spectra discussed earlier in connection with Fig. 3 above. It was pointed out that the Si 1s core-level spectra can be fitted well with a fairly symmetric peak shape, but that this is not the case for the Fe 1s spectra, especially for small x. The intensity of peak B, which lies on the higher binding-energy side of the Fe 1s spectrum, gradually decreases with increasing x. Peak B could be a satellite structure resulting from the electrostatic interaction between the created core hole and the valence electrons. Another possibility is that it originates from the presence of different chemical environments of inequivalent Fe sites. We comment further on these two mechanisms in the following.

It is well known that, owing to the coupling between core hole and valence orbitals, the core-polarization multiplets can produce a satellite structure. The key parameter here is the exchange splitting between the spins of core hole and valence electrons, which for an s core hole is described within a simple model as[25,35]

$$\Delta E_s = \left(\frac{2S+1}{2l+1}\right) G^l(s,l), \tag{3}$$

where $G^l(s,l)$ is the exchange integral and S is the total valence-electron spin; s denotes the s shell and l the valence

TABLE II. Some two-electron exchange integrals $G^l(s,l)$ of Fe and V atoms (after Ref. 36).

Element	$G^l(s,l)$	Value (eV)
Fe	$G^2(1s, 3d)$	0.046 571
	$G^2(2s, 3d)$	3.927 882
	$G^2(2p, 3d)$	4.255 168
	$G^2(3s, 3d)$	11.391 147
V	$G^2(1s, 3d)$	0.027 6120
	$G^2(2s, 3d)$	2.661 6928
	$G^2(2p, 3d)$	2.940 6906
	$G^2(3s, 3d)$	9.233 2683

orbital momenta. The intensity ratio in this model is proportional to the ratio of angular-momentum multiplicity, $S/(S+1)$. From the typical exchange integrals $G^l(s, l)$ of Fe and V free atoms listed in Table II (after Ref. 36), one finds that the exchange integral $G^2(1s, 3d)$ is far smaller than $G^2(3s, 3d)$. For example, in the case of bcc Fe, the typical $3s$ exchange splitting is of the order of 5 eV, while the $1s$ exchange splitting is of the order of 0.02 eV, being far smaller than the splitting between the peaks *A* and *B* (see Table I). This implies that the multiplet structure will mainly contribute to the broadening or asymmetry of the main peak. Moreover, the gradual reduction in the intensity ratio of the peak *B* to *A* for Fe $1s$ and the increase in the intensity ratio of the peak *B* to *A* for V $1s$ ($x>0.6$) cannot be explained by the exchange splitting.

The peak *B* can be interpreted to be due to the presence of two different Fe sites in $Fe_{3-x}V_xSi$. As seen in Fig. 4, the first-principles calculations predict that the Fe_I $1s$ core level lies at a higher binding energy of about 0.5 eV compared to Fe_{II}, which is consistent with assigning peak *B* with Fe_I sites. Our observation that the *B* to *A* intensity ratio in the spectra more or less tracks the concentration of Fe_I sites further supports this conclusion.

It is interesting that peak *B* displays a larger asymmetry than *A* (see Fig. 3 and Table I). The asymmetry of the core-level spectrum results not only from the multielectron excitations near the Fermi energy but also from the electrostatic interaction between the core hole and valence electrons.[25] As already noted, the relevant Fe $1s$ exchange integral is much smaller than that for Fe $3s$ (Table II), and will thus generate only a small spectral asymmetry, and the origin of this asymmetry is unclear. The Fe $1s$ spectrum has not been well studied so far due to the lack of availability of excitation energies to probe such a deep core level. As reference, we have measured Fe $1s$ spectra of bcc Fe and $Fe_{0.5}Co_{0.5}Si$ alloy, where the magnetic moments of bcc Fe and $Fe_{0.5}Co_{0.5}Si$ are known to be $2.2\mu_B$ and below $0.2\mu_B$ per Fe atom.[37] The spectra and the fitted results are shown in the inset of Fig. 3(a) and Table I. The estimated asymmetry parameters are 0.4 and 0.1 for bcc Fe and $Fe_{0.5}Co_{0.5}Si$, respectively. The asymmetry parameter of bcc Fe is thus similar to that of Fe_I, while the asymmetry parameter of $Fe_{0.5}Co_{0.5}Si$ is comparable to that of Fe_{II} site in $Fe_{3-x}V_xSi$. Recalling the reported magnetic moments of Fe_I and Fe_{II} sites of $2.5-3\mu_B$ and $1.2-0.3\mu_B$,[6–8,18,33] respectively, this suggests that the asymmetry parameter for Fe $1s$ spectrum scales with the Fe $3d$ magnetic moment.

In Table I, one also finds that peak *B* possesses substantial intensity for $x>0.6$, and especially for $x=1$, where we would expect no Fe_I contribution in the absence of compositional disorder in the system. At $x=1$, we observe 9% contribution from peak *B*, which is more or less consistent with the Fe and V disorders estimated by neutron diffraction.[6,8] This result indicates that the compositional disorder occurs in that the V atoms enter the Fe_{II} sites. Furthermore, for the V $1s$ spectrum, the *B* component contribution is zero or very small for $x<0.6$ but it is enhanced as the V content increases beyond this value. Incidentally, since Fe_{II} is more electronegative than Fe_I, the peak position of disordered V atoms on Fe_{II} site should be at lower binding energy, which is consistent with the position of the fitted peak *B* of V $1s$ core level.

IV. CONCLUSIONS

We have investigated the core-level photoemission spectra of $Fe_{3-x}V_xSi$ alloys over the entire V composition range via high-resolution HX-PES. We focus particularly on the Fe, V, and Si $1s$ core levels and find that all these core levels shift to higher binding energies with increasing V concentration. In comparing the measured core-level shifts as a function of doping with the corresponding predictions of the first-principles, all electron computations within the framework of the LSDA, a reasonable overall level of agreement is found although the size of the computed shifts for Fe_I and V is larger than the measured values. The discrepancies between theory and experiment can be ascribed to the effect of core-hole screening in the photoexcitation process, which is not accounted for in the computations. Our analysis shows that the shift of the core levels of Fe, V, and Si to higher binding energies with increasing V content is caused mainly by the shift of the chemical potential to higher energies as a pseudogap is formed around the Fermi level in the electronic spectrum of the alloy.

ACKNOWLEDGMENTS

This work was done under the approval of the SPring-8 Proposal Assessing Committee (Proposal No. 2005B3811) and was also supported by the Ministry of Education, Culture, Sports, Sciences and Technology of Japan. The analyzer development was supported by SENTAN, JST. We acknowledge Y. Nishino, K. Tamasaku, and T. Ishikawa, members of RIKEN for their excellent tuning of the beamline BL29XU. It is a pleasure to acknowledge important discussions with Peter Mijnarends. The work at Northeastern University was supported by the Division of Materials Science and Engineering, Office of Basic Energy Science, U.S. Department of Energy, under Contract No. DE-FG02-07ER46352, and benefited from the allocation of time at the NERSC supercomputing center and Northeastern University's Advanced Scientific Computation Center (ASCC).

*Present address: Hiroshima Synchrotron Radiation Center, Hiroshima University, Higashi-Hiroshima 739-0046, Japan.
†akiok@hiroshima-u.ac.jp

[1] Y. Nishino, S. Y. Inoue, S. Asano, and N. Kawamiya, Phys. Rev. B **48**, 13607 (1993).
[2] Y. Kawaharada, H. Uneda, K. Kurosaki, and S. Yamanaka, J. Alloys Compd. **359**, 216 (2003).
[3] J. J. Jia, T. A. Callcott, W. L. O'Brien, Q. Y. Dong, D. R. Mueller, D. L. Ederer, Z. Tan, and J. I. Budnick, Phys. Rev. B **46**, 9446 (1992).
[4] O. Nashima, T. Kanomata, Y. Yamaguchi, S. Abe, T. Harada, T. Suzuki, H. Nishihara, K. Koyama, T. Shishido, K. Watanabe, and T. Kaneko, J. Alloys Compd. **383**, 298 (2004).
[5] K. Soda, H. Murayama, K. Shimba, S. Yagi, J. Yuhara, T. Takeuchi, U. Mizutani, H. Sumi, M. Kato, H. Kato, Y. Nishino, A. Sekiyama, S. Suga, T. Matsushita, and Y. Saitoh, Phys. Rev. B **71**, 245112 (2005).
[6] T. J. Burch, J. I. Budnick, V. A. Niculescu, K. Raj, and T. Litrenta, Phys. Rev. B **24**, 3866 (1981).
[7] A. Bansil, S. Kaprzyk, P. E. Mijnarends, and J. Tobola, Phys. Rev. B **60**, 13396 (1999).
[8] J. Kudrnovský, N. E. Christensen, and O. K. Andersen, Phys. Rev. B **43**, 5924 (1991).
[9] A. C. Swintendick, Solid State Commun. **19**, 511 (1976).
[10] S. Ishida, J. Ishida, S. Asano, and J. Yamashita, J. Phys. Soc. Jpn. **21**, 53 (1976).
[11] S. Fujii, S. Ishida, and S. Asano, J. Phys. Soc. Jpn. **64**, 185 (1995).
[12] S. Ishida, S. Akazawa, Y. Kubo, and J. Ishida, J. Phys. F: Met. Phys. **12**, 1111 (1982).
[13] S. Fujii, S. Sugimura, S. Ishida, and S. Asano, J. Phys.: Condens. Matter **2**, 8583 (1990).
[14] K. Ullakko, J. K. Huang, C. Kantner, R. C. O'Handley, and V. V. Kokorin, Appl. Phys. Lett. **69**, 1966 (1996).
[15] K. Koyama, H. Okada, K. Watanabe, T. Kanomata, R. Kainuma, W. Ito, K. Oikawa, and K. Ishida, Appl. Phys. Lett. **89**, 182510 (2006).
[16] By pseudogap we simply mean a region of reduced electronic density of states, which arises in the one-particle spectrum within the band theory computations discussed in this paper. This should not be confused with the controversies surrounding the pseudogap phenomena in strongly correlated systems such as the cuprate high-temperature superconductors.
[17] N. F. Mott and H. Jones, *The Theory of the Properties of Metals and Alloys* (Dover, New York, 1958).
[18] V. A. Niculescu, T. J. Burch, and J. I. Budnick, J. Magn. Magn. Mater. **39**, 223 (1983), and references therein.
[19] Y. T. Cui, A. Kimura, K. Miyamoto, K. Sakamoto, T. Xie, S. Qiao, M. Nakatake, K. Shimada, M. Taniguchi, S.-i. Fujimori, Y. Saitoh, K. Kobayashi, T. Kanomata, and O. Nashima, Phys. Status Solidi A **203**, 2765 (2006).
[20] H. Kitamura, Rev. Sci. Instrum. **66**, 2007 (1995).
[21] H. Kitamura, J. Synchrotron Radiat. **7**, 121 (2000).
[22] C. R. Brundle, J. Vac. Sci. Technol. **11**, 212 (1974).
[23] K. Kobayashi, M. Yabashi, Y. Takata, T. Tokushima, S. Shin, K. Tamasaku, D. Miwa, T. Ishikawa, H. Nohira, T. Hattori, Y. Sugita, O. Nakatsuka, A. Sakai, and S. Zaima, Appl. Phys. Lett. **83**, 1005 (2003); Y. Takata, M. Yabashi, K. Tamasaku, Y. Nishino, D. Miwa, T. Ishikawa, E. Ikenaga, K. Horiba, S. Shin, M. Arita, K. Shimada, H. Namatame, M. Taniguchi, H. Nohira, T. Hattori, S. Södergren, B. Wannberg, and K. Kobayashi, Nucl. Instrum. Methods Phys. Res. A **547**, 50 (2005); K. Kobayashi, *ibid.* **547**, 98 (2005).
[24] It was confirmed that the peak position at the maxima for Fe and V 2*p* core levels and the fitted peak position of peaks *A* and *B* show the same trends as shown in Fig. 4.
[25] S. Hüfner, *Photoelectron Spectroscopy*, 3rd ed. (Springer-Verlag, Berlin, 2003), Chap. 2.
[26] M. Cardona and L. Ley, *Photoemission in Solids I* (Springer-Verlag, Berlin, 1978), Chap. 1.
[27] K. Hübner, Phys. Status Solidi A **42**, 501 (1977).
[28] A. Ino, T. Mizokawa, A. Fujimori, K. Tamasaku, H. Eisaki, S. Uchida, T. Kimura, T. Sasagawa, and K. Kishio, Phys. Rev. Lett. **79**, 2101 (1997).
[29] A. Fujimori, A. Ino, J. Matsuno, T. Yoshida, K. Tanaka, and T. Mizokawa, J. Electron Spectrosc. Relat. Phenom. **124**, 127 (2002).
[30] Since our computations are not fully relativistic, the theoretical values in Figs. 4 and 5 have been obtained by averaging the shifts for the various (relativistic) core levels for the up- and down-spin computations.
[31] In defining the CPS in Fig. 5, we have taken the bottom of the valence band as the common energy zero for various alloy compositions. This definition of the chemical potential however is not unique.
[32] L. P. Bouckaert, R. Smoluchowski, and E. Wiger, Phys. Rev. **50**, 58 (1936).
[33] A. R. Williams, V. L. Moruzzi, C. D. Gelaatt, J. Kübler, and K. Schwartz, J. Appl. Phys. **53**, 2019 (1982).
[34] I. Galanakis, P. H. Dederichs, and N. Papanikolaou, Phys. Rev. B **66**, 174429 (2002).
[35] J. H. van Vleck, Phys. Rev. **45**, 405 (1934).
[36] J. B. Mann, Los Alamos Scientific Laboratory Report No. LA-3690, 1967.
[37] J. Guevara, V. Vildosola, J. Milano, and A. M. Llois, Phys. Rev. B **69**, 184422 (2004).